Aeroelastic coupling in sonic boom optimization of a supersonic aircraft

Mariano Vázquez, Alain Dervieux, Bruno Koobus

INRIA

INSTITUT NATIONAL DE RECHERCHE EN INFORMATIQUE ET EN AUTOMATIQUE

Aeroelastic coupling in sonic boom optimization of a supersonic aircraft

M. Vázquez A. Dervieux B. Koobus

N° 4865

June 26th, 2003

THÈME 1

ISSN 0249-6399 ISRN INRIA/RR--4865--FR+ENG

INRIA
SOPHIA ANTIPOLIS

Aeroelastic coupling in sonic boom optimization of a supersonic aircraft

M. Vázquez* A. Dervieux† B. Koobus‡

Thème 1 — Réseaux et systèmes
Projet Tropics

Rapport de recherche n° 4865 — June 26th, 2003 — 26 pages

Abstract: In this paper, we consider a multi-disciplinary optimization problem where the initial shape of a wing is sought in order to cope, after elastic deformation by the flow, with some optimality conditions. We propose a medium-strong coupling which allows to consider different softwares communicating a small number of times. Applications to the optimization of the AGARD Wing 445.6 and a flexible supersonic aircraft wing are presented.

Key-words: Computational fluid dynamics - Shape optimal design - Gradient method - Shape parametrization - Steepest descent - Optimization - Multilevel optimization - Adjoint methods - Euler equations - Unstructured mesh - Transpiration conditions - Fluid/Structure interaction

* GRIDSYSTEMS, Parc Bit - Son Espanyol, 07120 Palma de Mallorca, Baleares, Spain, and INRIA
† INRIA, 2004 Route des Lucioles, BP. 93, 06902 Sophia-Antipolis, France
‡ Université de Montpellier II, Dept Mathématiques, CC.051, 34095 MONTPELLIER Cedex 5, France, and INRIA

Unité de recherche INRIA Sophia Antipolis
2004, route des Lucioles, BP 93, 06902 Sophia Antipolis Cedex (France)
Téléphone : +33 4 92 38 77 77 — Télécopie : +33 4 92 38 77 65

Couplage aeroelastique et optimization du bang sonique pour un avion supersonique

Résumé : Nous considérons le problème de l'optimisation multi-disciplinaire dans lequel on cherche une forme d'aile au repos qui, après déformation par l'écoulement, sera optimale selon certains critères. Nous proposons un couplage semi-fort qui permet d'associer différents logiciels qui communiqueront seulement un petit nombre de fois. On présentera des applications à l'optimisation de l'aile d'un avion supersonique souple et de l'aile AGARD 445.6.

Mots-clés : Mécanique des Fluides Numérique - Optimisation de forme - Méthode de gradient - Paramétrisation de forme - Plus grande descente - Optimisation - Optimisation multi-niveau - Équations d'Euler - Maillage non-structuré - Conditions de transpiration- Interaction Fluide/Structure

1 Introduction

Many algorithms are proposed in the literature for optimizing the shape of an aircraft under aerodynamical analysis. In real life, the shape of wings of an aircraft are not completely decided by the design, since when on the ground, wings are deformed under the action of their weight . In flight, wings are deformed by aerodynamic forces, that are at least as large as the weight of the complete aircraft.

Following [1], the links between aircraft aerodynamics and structural response are basically two. Firstly, aeroelastic deformations significantly change the flow around the aircraft. And secondly, the structural weight acts directly on its lift and drag. To compensate the first effect, a normal industrial practice is to design the shapes using a jig-shape approach, that is considering a priori the aeroelastic deformations to produce the desired shape. This can be done by substracting the aeroelastic deformation from the optimal cruise shape. This leaves only the second link active, that is just the weight of the structures. At first sight, this simplifies the coupled aeroelastic optimization. In the field of **Multidisciplinary Optimization (MDO)** any simplification is welcome because of the dramatic complexity of aircraft design (see the authoritative [2]). However, jig-shape corrections are in some case inaccurate approximations, and they are likely to fall short in the case of multipoint optimisation since several flow regimes would provide several corrections and thus not a unique shape. An enlightening example concerns supersonic jets optimisation, where a trade-off between subsonic and supersonic regimes design has to be done.

The purpose of this work is to propose a method which couples directly fluid and structure, and which is, for this reason, able to be extended to multiple point situations.

A direct approach consists of an optimisation loop around a fully coupled solver, combining fluid and structure effects. It is necessary then to efficiently compute the sensitivity of the coupled model. Its evaluation for aeroelastic coupling is a very complex matter (see for instance [3, 4, 5]). This problem is common to all MDO domain: the need to evaluate the dependence between the different disciplines acting in the optimization process, which is expressed through the objective function (i.e. the cost we want to minimize). For instance, in the case of aeroelastic-aerodynamic coupling, it typically contains aerodynamic performance or flight condition related terms (lift/drag, sonic boom production, incidence angle, etc.) and it may contain also structural ones (internal stresses, elastic model parameters, etc.). In [5], this sensitivity evaluation is simplified using a reduced model for the structural behaviour based on the Global Sensitivity Equations (GSE) proposed in [6]. The idea is to evaluate the total sensitivity derivatives linking loads and deformations using a modal decomposition of the static aeroelastic response. This approach is also followed in [7]. In all of these cases, the optimization runs both on the aerodynamic and the aeroelastic sides. When both models, flow and elasticity need to be accurate ones, this kind of approach is rather heavy in terms of developement and computational costs.

Then, we might wish a method that is more accurate than the simplified jig-shape method, in particular, if the final purpose is to obtain a multi-point optimization. At the same time, the method might be less heavy than a tightly coupling method. It could consist of an appropriate not too strong iterative coupling between the optimization step and the

fluid-structure analysis. This should be possible in the frequent case where the optimal deformed geometry does not depend on structure features, i.e. the global optimization system can be well approximated as an optimal deformed shape problem to be post processed by a structural inverse problem.

In our approach, we shall consider an **interior** optimization loop and an **exterior** coupling cycle, which is an aeroelastic analysis over the current iteration's optimized shapes. This line is also followed by [8], who use a parametric or "CAD-based" formulation (according to the terminology of [9]). In contrast to that work, in the present paper, the shape is not subject to a CAD parametrization (in other words our approach is "CAD-free"). Since in this case shape modifications and aeroelastic deformations are represented in a similar manner, our option is favourable to an easier coupling of them. In particular, we shall be able to superpose these modifications in a way very similar to linearization. This may result in an iteration that combines a non-weak coupling and yet a small computer power consuming and a non-complex software development.

In order to propose a rather simple implementation of this principle, we shall optimise with a fixed mesh, and only aeroelasticity analysis will need a dynamic mesh.

- The aeroelastic response is computed on dynamic meshes from the optimized shape obtained at the previous coupling iteration with a loosely coupled unsteady scheme, described in details in [10].

- A fixed-domain shape optimizer using transpiration conditions and a "CAD-free" approach, introduced in [11, 12], will be in turn applied to the previous aeroelastic deformed shape in order to optimise aerodynamic performances.

We shall apply these principles to the analysis of the influence of aeroelastic deformations in Optimal Shape Design problem accounting not only for the lift/drag point of view but also for **sonic boom optimization**, which is of utmost importance for future supersonic civil jets. We shall concentrate on two situations: at rest, (no forces act on the structure, we do not consider gravity effects) and at cruise flight for which we consider that steady aerodynamic forces act on the structure (and again gravity effects are not considered).

We end this introduction with a few words about our model for sonic boom. Sonic boom is the ground signature of the pressure shock produced by an aircraft flying at supersonic speed [13]. Any solid body moving at supersonic speed develops a shock ahead that moves with it. For airplanes, this feature becomes a complex shock system (Figure 1). But no matter how complex it is, several airplane lengths below it coalesces, ultimately arriving at the soil as a (single or composite) N-shape function. This ground signature is responsible for structural damage in buildings, strong environmental impact, psychological effects on human beings in the area, and so on. It is not possible to escape to sonic boom production (except for no-lift bodies, which are not an issue of aircraft industry...) because lift force has to be transmitted to the ground. But many solutions have been proposed to reduce it directly or to reduce its effects. In [11, 12] we have proposed to use optimal shape design to reduce what we call **Sonic boom downwards emission (SBDE)**. SBDE is the pressure gradient strength, measured as a volume integral inside a "box" right below the aircraft, namely it corresponds to the **near field** pressure shock system.

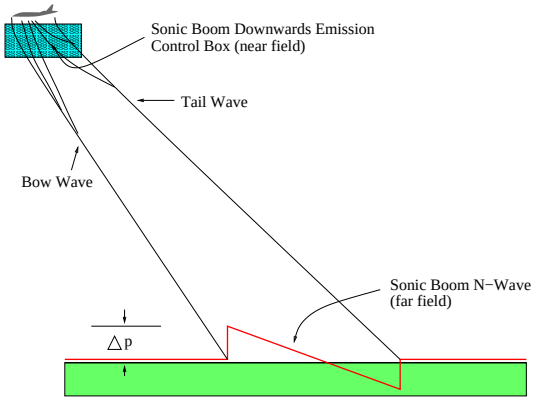

Figure 1: The sonic boom. Sketch of near and far field shock wave patterns of a supersonic aircraft.

2 A three modules scheme

The coupled aerodynamic-aeroelastic optimization problem involves two main phases, that repeat iteratively until a convergence criteria is achieved. To an **aeroelastic analysis** phase follows an **aerodynamic optimization** stage. Each phase corresponds to a different module.

The topology of our meshes is held constant during the whole process, so that meshes will be only the object of deformations. The various shapes are represented in two different manners. A "Volumic Shape" contains the coordinates of the whole 3D volumic mesh. It is typically denoted by $\Omega \in \mathbb{R}^{3\times N^{\text{vol}}}$ where N^{vol} is the total number of nodes in the volume mesh. A "Skin Shape" is given by the skin mesh coordinates of the aircraft. We denote it $\gamma \in \mathbb{R}^{3\times N^{\text{skin}}}$, where N^{skin} is the total number of mesh nodes that lie on the boundary corresponding to the wing shape.

It appears then necessary to be able to transform easily a type of data into the other one. To this end, and as an interface between the two above modules, the proposed algorithm involves a module that generates the mesh equivalent to the transpired optimised shape. The **remeshing module** both organises the communication between the other modules and enhances the accuracy of the transpiration-based optimisation by replacing the transpiration model by a genuine deformed-mesh one.

The three main tools are sketched as follows:

- **The aeroelastic analysis module:** a loosely coupled fluid-structure solver $\Phi(\Omega, \Sigma)$.
- **The aerodynamic optimization module:** an aerodynamic optimizer $\Upsilon(n, \Omega)$.
- **The remeshing module:** a remeshing tool $\Xi(\gamma, \Omega)$.

We will also distinguish the meshes *at rest* from the **cruise** ones, noted $\widehat{\Omega}$ and $\overline{\Omega}$ respectively. The former ones are equivalent to the shapes at rest, optimized or not. The cruise meshes are those following the shape aeroelastic deformations, also optimized or not. By saving separately optimization and aeroelastic modifications, one can recover the original shapes at the end of the coupled optimization. An additional input item is $\Sigma \in \mathbb{R}^{3\times N^{\rm stru}}$. It corresponds to the structure grid which is, in our case, a thin plate embedded in the considered wing. The structural model is a linear one, like that of [7, 10]. Typically, $N^{\rm stru} << N^{\rm vol}$, which makes the structural problem much smaller and cheaper to solve than the fluid dynamics one. The grid notation is summarized as follows: the **volume meshes at rest** are noted $\widehat{\Omega}$, the **structure meshes at rest** are noted $\widehat{\Sigma}$ and the **cruise volume meshes** are noted $\overline{\Omega}$. Let us depict each of the modules.

2.1 The aeroelastic analysis module $\Phi(\hat{\Omega}, \hat{\Sigma})$

Fluid-Structure Solver $\Phi(\hat{\Omega}, \hat{\Sigma})$

Inputs:

$\widehat{\Omega} \in \mathbb{R}^{3\times N^{\rm vol}}$, fluid mesh *at rest*

$\widehat{\Sigma} \in \mathbb{R}^{3\times N^{\rm stru}}$, structure flat plate mesh *at rest*

Output:

$\overline{\Omega} \in \mathbb{R}^{3\times N^{\rm vol}}$, *cruise* fluid mesh

`Compute the deformed fluid mesh` $\overline{\Omega}$`, coming from the fluid-structure coupling:`

$$\overline{\Omega} = \Phi(\widehat{\Omega}, \widehat{\Sigma})$$

The aeroelastic module is based on the methodology introduced in [10, 14]. The solution of the coupled fluid-structure problem is computed by a staggered solution procedure in time [15]. This scheme is also used in [7] for computing the aeroelastic response. This kernel yields a coupled fluid-structure static analysis based on a pseudo time advancing scheme with two stages: a fluid evaluation stage followed by a structural computation, based on the pressure distribution given by the preceding fluid simulation. First, at the fluid stage, a mesh conforming to the structure deformation is built by moving the vertices with a pseudo-

structural model [16]. Then the flow is advanced on this mesh. The spatial discretization of the compressible flow Euler equations is based on a finite volume method, using a second order space accurate scheme based on the Roe solver. For addressing the problem of the flow simulation on moving grids, an Arbitrary Lagrangian Eulerian formulation is incorporated in the flow solver (in the present case of static coupling, this is not essential when the mesh is moving from the current position to the next one). Next, at the structural stage, the pressure loads are applied to the structure and the resulting displacements are computed. The structure is represented by a finite element model of a flat plate, embedded in the wing, which is a simplified model of the internal structure. The displacements are finally transferred to the wet surface of the wing, producing a deformed volume mesh. After convergence towards the static aeroelastic response, this volume mesh, is the output of the aeroelastic analysis module.

2.2 The aerodynamic optimization module $\Upsilon(n, \bar{\Omega})$

Aerodynamic Optimizer $\Upsilon(n, \bar{\Omega})$

Inputs:

n, number of optimization iterations

$\overline{\Omega} \in \mathbb{R}^{3 \times N^{\text{vol}}}$, cruise fluid mesh

Output:

$\gamma_n \in \mathbb{R}^{N^{\text{skin}}}$, shape correction

`Do` $nc = 1, n$

- `Compute state` $W(\overline{\Omega})$ `and adjoint` $\Pi(\overline{\Omega})$`, compute the gradient` $g(\gamma_{nc}, W(\overline{\Omega}), \Pi(\overline{\Omega}))$
- `Compute the preconditioner` P^*
- `Compute` ρ `(internal cycle)`
- `Update the shape correction:`

$$\gamma_{nc} = \gamma_{nc-1} - \rho \quad P^* \; g(\gamma_{nc}, W(\overline{\Omega}), \Pi(\overline{\Omega}))$$

`Next` nc

The aerodynamic optimizer is based on what was first proposed in [11, 12]. It is a **CAD-Free** based algorithm: the design parameters space is set by the physical positions of each of the skin discretization nodes placed on the shape to be optimized. Here, the shapes derived from the iterative optimization process are characterized using a **transpired perturbation**, noted as γ. According to this, a scalar which corresponds to a (small) displacement in the normal direction is assigned to each skin node. Therefore $\gamma \in \mathbb{R}^{N^{\text{skin}}}$, where N^{skin} is the number of skin nodes on the optimization's target shape. High frequency effects in space are dramatically reduced by using a multilevel preconditioner applied to the shape gradient. In order to cope with the probably very large number of parameters defining the target shape, an adjoint problem is built (see [17]). We have chosen to use a **discrete adjoint** ([18], [19]). The optimization algorithm in [11, 12] was designed to reduce the **sonic boom downwards emission** while preserving some target aircraft performance properties, basically lift and/or drag.

The optimizer inputs are the number n of optimization iterations and a given initial volume mesh Ω. As for the aeroelastic analysis module, the optimizer works unaware of the situation of the input mesh: it could be either a mesh at rest $\widehat{\Omega}$ or a cruise one $\overline{\Omega}$. We have designed the full scheme considering that the input mesh of the optimizer is a cruise one $\overline{\Omega}$. Indeed, it is expected that the surface deformations related to the optimization will be smaller than those coming from the aeroelastic coupling. So the optimizer starts from a given cruise mesh $\overline{\Omega}$ that remains unchanged all along its way until the end of the current optimization cycle.

After n iterations, a γ_n is obtained. It represents a displacement of the boundary defining an optimum shape by means of the transpiration conditions (like in [20] for instance). For each iteration nc, firstly the state $W(\overline{\Omega})$, its adjoint $\Pi(\overline{\Omega})$ state and the cost functional gradient $g(\gamma_{nc}, W(\overline{\Omega}), \Pi(\overline{\Omega}))$ are computed. In order to get $W(\overline{\Omega})$, the discretized **compressible flow Euler equations** are solved by means of a finite volume method and integrated using a second order space accurate Roe upwind scheme. The cost functional gradient is then calculated. The original cost functional was proposed in [11]. Here we have introduced some modifications to render it more efficient. It evaluates both the aerodynamic properties and what we call the sonic boom downwards emission (SBDE):

$$j(\gamma) = \alpha_1 \ {f_D}^2 + \alpha_2 \ {f_L}^2 + \alpha_3 \int_{\overline{\Omega}^B} \frac{\partial p}{\partial x_i} \frac{\partial p}{\partial x_i} \ dV \tag{1}$$

where

$$f_D = \begin{cases} C_D - C_D^{target} & \text{if } C_D \geq C_D^{target} \\ 0 & \text{otherwise} \end{cases}$$

$$f_L = \begin{cases} C_L - C_L^{target} & \text{if } C_L \leq C_L^{target} \\ \\ 0 & \text{otherwise} \end{cases}$$

and α_1, α_2 and α_3 are constants that allow to vary the relative weight between the cost functional terms. These terms are related respectively to the aerodynamical performance (drag, lift) and SBDE. The integration volume $\overline{\Omega}^B$ is a control box defined as a part of the computational domain located below the airplane. The functions f_D and f_L are zero when the drag is smaller than the target drag and when the lift is larger than the lift target, respectively.

The shape volume is conserved by sections, projecting the gradient on a volume preserving space [11]. In order to avoid volume "migration" from one end to the other for the optimized shapes, the whole volume can be divided in a certain number of sections, in general transversal to the spanwise direction. Therefore, each node i can be assigned to a section which contains $N(i)$ of them. The volume is then preserved individually for each of the sections.

In order to satisfy at best a lift condition, we have implemented a variable incidence equation, based on that of [21]. At each iteration n, the incidence angle θ is updated according to

$$\theta^{nc+1} = \theta^{nc} - \frac{1}{2}\, f_L^{nc}. \tag{2}$$

It makes use of the linear dependence between the incidence angle and the lift coefficient for small incidences. The incidence angle is increased between two optimization iterations *only* when the lift is smaller than the target lift, namely when cambering fails to recover it.

2.3 The remeshing module $\Xi(\gamma_n^p, \overline{\Omega}^p)$

Remeshing Algorithm $\Xi(\gamma_n^p, \overline{\Omega}^p)$

Inputs:

$\gamma_n^p \in \mathbb{R}^{N^{\text{skin}}}$, optimised shape correction at iteration p

$\overline{\Omega}^p \in \mathbb{R}^{3 \times N^{\text{vol}}}$, cruise fluid mesh

Output:

$\overline{\Omega}^p_{\text{OPT}} \in \mathbb{R}^{3 \times N^{\text{vol}}}$, optimised cruise fluid mesh

`Move the input mesh` $\overline{\Omega}^p$ `according to` γ^p`:`

$$\overline{\Omega}^p_{\text{OPT}} = \Xi(\gamma_n^p, \overline{\Omega}^p)$$

The remeshing module works as an interface between the aeroelastic module and the optimization one. The aeroelastic module already includes the same remeshing algorithm to take into account the shape deformations. They are transferred to the optimization module as a modified volume grid, called the cruise mesh $\overline{\Omega}^p$ for a coupling iteration p, suitable to be the optimizer input. On the other hand, the optimizer's output is a shape correction γ_n^p defined on the surface nodes according to the transpiration condition. Through a remeshing algorithm (e.g. [15] and [16]), a corrected volumic grid is produced, which will be used in turn as input by the aeroelastic module. The algorithm generates a new mesh by moving the nodes of the input mesh $\overline{\Omega}^p$ with a pseudo-structural model, under the constraint that the new boundary nodes are moved from the input ones according to the input shape correction γ_n^p.

3 Coupling algorithm

Optimization + Aeroelastic Coupling Algorithm

$\widehat{\Omega}^0$ = initial (optimized) mesh at rest

Do p (coupling iterations)

- Compute the aeroelastic coupling from the fluid mesh *at rest* $\widehat{\Omega}^{p-1}$ and structure mesh $\widehat{\Sigma}$, and obtain the intermediate *cruise* mesh $\overline{\Omega}^p$:

$$\overline{\Omega}^p = \Phi(\widehat{\Omega}^{p-1}, \widehat{\Sigma})$$

- Compute the optimum boundary correction γ_n^p by optimizing $\overline{\Omega}^p$, through n optimization iterations:

$$\gamma_n^p = \Upsilon(n, \overline{\Omega}^p)$$

- Compute the optimized *cruise* mesh $\overline{\Omega}^p_{\text{OPT}}$:

$$\overline{\Omega}^p_{\text{OPT}} = \Xi(\gamma_n^p, \overline{\Omega}^p)$$

- Evaluate the optimized mesh *at rest*, namely $\widehat{\Omega}^p_{\text{OPT}}$:

$$\begin{aligned} \Delta\widehat{\Omega}^p_{\text{OPT}} &= \overline{\Omega}^p_{\text{OPT}} - \overline{\Omega}^p \\ \widehat{\Omega}^p_{\text{OPT}} &= \widehat{\Omega}^{p-1} + \Delta\widehat{\Omega}^p_{\text{OPT}} \end{aligned}$$

- Set $\widehat{\Omega}^p = \widehat{\Omega}^p_{\text{OPT}}$

Next p

In the proposed coupling algorithm, there are two nested iterative cycles: a global **coupling cycle** and a nested **optimization cycle**. In the coupling cycle, the *Aeroelastic Module* Φ evaluates the shape's structural response to the surface pressure distribution, i.e. it computes the **cruise** configuration from the one *at rest*. Then, the *Optimization Module* Υ modifies the cruise shape coming from Φ by performing n optimization iterations. That is to say, it optimizes the cruise configuration as if it were rigid and only submitted to SBDE and

aerodynamics constraints. It produces a shape modification γ. The *Remeshing Module* Ξ is applied to transform the transpired shape modifications γ in a volume grid. The new shape at rest is obtained by updating the previous one with the difference between the optimized cruise shape and the current cruise shape. The new shape at rest is in turn given as non-deformed geometry to the *Aeroelastic Module* to start a new iteration $p+1$. For a faster convergence, this process is initiated by a synthesis of non-deformed geometry and of the previous elastic deformation.

From the implementation side, we have observed that, at each coupling iteration p, it is very advantageous to keep the optimization modifications corresponding to iteration $p-1$ to evaluate the optimized $\gamma_n^p = \Upsilon(n, \overline{\Omega}^p)$. In this way Υ's input $\overline{\Omega}^p$ corresponds to the $p-1$ optimized shape with the corresponding p aeroelastic deformation. The starting point for the current Υ cycle is therefore closer to the following optimized state.

After n optimization iterations that introduce surface modifications γ_n through transpiration conditions, the *Remeshing Module* Ξ is called to deform the whole mesh while keeping the original topology. Then, Φ and Υ can be linked. As a bonus, their output mesh deformations can be saved independently at each iteration to keep track of the separate effects of the aeroelasticity and the optimization. This is particularly important in order to see what is the final optimized shape of the aircraft at rest. The number of optimization iterations n can vary in order to improve the scheme's turnaround time. Indeed, a complete optimization convergence is not necessary in the first full scheme cycles.

By construction, the method that we propose is dedicated to find the optimal shape for the coupled fluid-structure system. Any fixed point of the algorithm will satisfy the optimality condition for the deformed shape. Furthermore, this optimality condition is checked by a mesh following the deformed geometry, and with, at convergence, a vanishing transpiration displacement. This implies that the transpiration approximation has only an influence on the optimality condition that is fulfilled, and not on the flow evaluation. Indeed, the flow evaluation does not suffer from transpiration inaccuracies since, with a zero displacement at convergence, the transpiration condition reduces to the usual slip boundary condition.

4 Numerical Examples

The proposed scheme is now evaluated through two concrete optimization problems. We shall focus on two issues.

On one hand, the scheme must be **convergent** in the sense that, as the coupling iterations go on, the otained geometries should converge to a limit shape. Both Φ and Υ deform shapes. That is to say Φ evaluates the structural response to a steady flow solution and Υ corrects the surfaces after a given minimization objective. The goal is that, at the end, each of Φ and Υ must not undo what the other one has previously done. A priori, this is not at all an obvious point. The negative twisting of the wings in flight produce (i) a lift loss and (ii) a SBDE reduction. Then, the optimization process will try to recover from (i) while keeping an eye on (ii). Point (i) could be compensated by two means: cambering

and incidence angle variation. But of course, this shape modification will have effects on the following structural response! We will show to what extent this combined effects are entangled.

On the other hand, it is obvious that the scheme must be **useful**. What is the interest in including the aeroelastic effects in an aerodynamical optimization process involving sonic boom reduction? Clearly, both torsion and flexion do have an effect on the aerodynamic performance. The point is to assess its effect on sonic boom reduction.

The examples shown are the sonic boom optimization of the AGARD wing 445.6 and of the delta wing of a Supersonic Business Jet projected by Dassault Aviation. For both cases, first we carry out some optimization iterations on the rigid wings, namely without aeroelastic deformations. The optimized (rigid) wings illustrate the performance of our sonic boom optimizer scheme and its ability to reduce the SBDE while keeping the aerodynamic properties. As a second stage, we start a coupled aerodynamic optimization / aeroelastic analysis computation for which the initial geometries are those optimized (rigid) wings. In the case of the AGARD wing, we evaluate the robustness of the scheme by considering a very flexible wing.

4.1 Dassault's Aviation Supersonic Business Jet wing

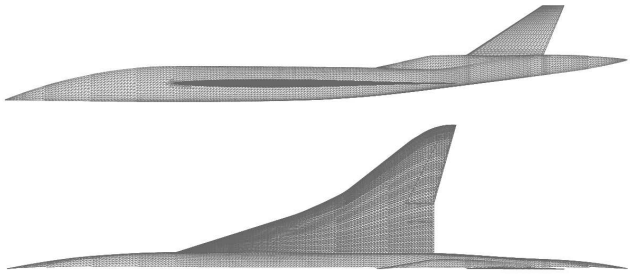

Figure 2: Dassault Aviation's Supersonic Business Jet. Side and upper views.

The first example is the sonic boom optimization of the wings of a Supersonic Business Jet (SBJ) projected by Dassault Aviation, whom we are indebted for providing the geometry (Figure 2). The aircraft isolated wings are depicted in Figure 3.

The baseline wings provided by the constructor for this generic geometry are horizontally symmetrical, with two different sweep angles of 17° and 38° respectively, and a rather smooth transition between them. The Mach angle for $M = 1.8$ is around 34°. Then, while the inboard part of the wings falls within the Mach cone (viz. [22]), producing a lower wave drag, the outboard wing cuts through the Mach cone. As a consequence, the sharpest pressure gradients are produced ahead of the outboard portion of the wing. The wing volume mesh corresponding to Figure 3 is made of 65418 tetrahedra (12963 nodes) and its surface

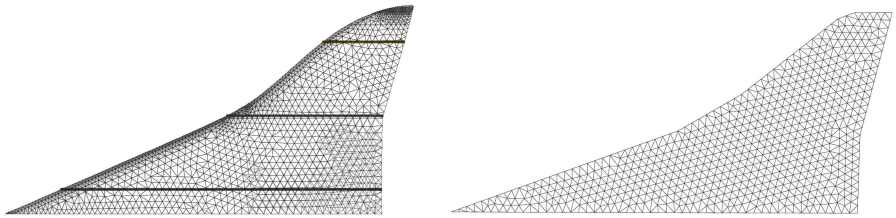

Figure 3: Dassault Aviation's Supersonic Business Jet. Left: Isolated wing discretization, showing the cross-sectional shapes (airfoils) considered (the thick horizontal lines): outboard, mid and inboard. Right: structural mesh (flat plate finite element model).

mesh contains 4692 triangles (2408 nodes). The Mach number is set to 1.8 and the initial incidence angle is 3°.

4.1.1 Initial rigid optimization

The double delta wing renders optimized shapes that are very different than those of more simple forms. The fact is that the wing inboard produces a much lower pressure gradient due to its sweep angle, which is smaller than that of the Mach cone. Therefore, while the shape modifications that reduce the SBDE tend to focus on the outboard half, the lift can be recovered by cambering the inboard region. This effect is naturally developed by our algorithm. After optimization, the wing profiles at different locations in the wing-span direction show different forms, depending on its position relatively to the fuselage. Figure 4 shows the three wing cros-sectional cuts of Figure 3, left. After 30 optimization cycles and using a **volume preserving projected gradient (VPGP)** strategy [11] that preserves the volume per-wingspan-section, the outboard profile develops a flattened downwards half and a sharp leading edge. On the other hand, in the inboard one this effect is much less evident. The mid-section profile shows a combination of those effects, stronger perhaps for the sonic boom reduction than for the lift recovery. Some very slight wiggles appear on the optimal shapes. that would be easily mastered with a smoother parametrization as in [23].

Figure 5 illustrates the SBDE reduction, as the pressure distribution in a plane below the wing. Note the pressure peak location for the original wings. As addressed in [11], this is a strong reason for not using a propagation code that only considers as input what happens in a line contained in the aircraft symmetry plane in order to evaluate the ground pressure signature . Unless one has a refined volume grid, adapted to follow the strong shock produced *below* the wing and *out of* the symmetry plane, the pressure signature so computed will be only that of the fuselage. This point leads us to believe that this kind of propagation methods present an important drawback: they are strongly sensitive to the position of the line used to take the input pressure distribution.

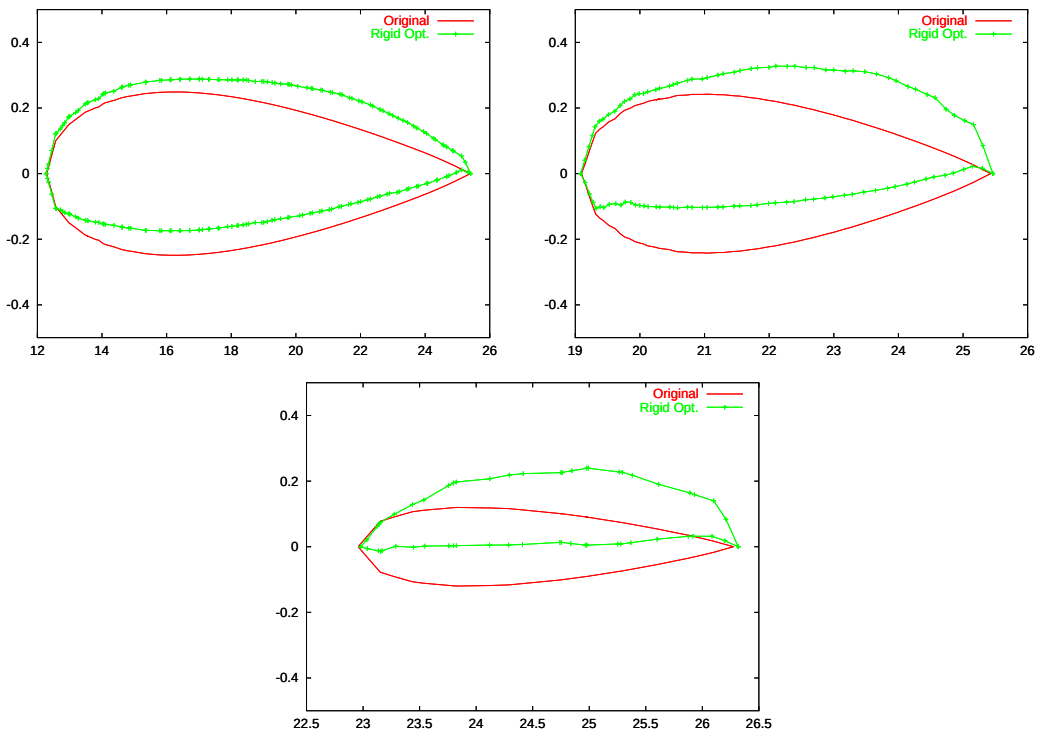

Figure 4: Dassault Aviation's Supersonic Business Jet. Non-coupled optimization of a rigid wing. From left to right and from top to bottom: inboard, midboard and outboard aircraft wing airfoils.

4.1.2 Optimization + Aeroelastic coupling

For the aeroelastic simulations, we use a thin plate finite element model of the wing which contains 1286 triangular shell elements (Figure 3, right). The properties of the material have been calibrated so that realistic eigenmodes and eigenvalues are recovered.

We proceed to compute the coupled optimization from the optimized rigid wing as starting point. As said above, the flexion and torsion of the delta wing is stronger in the outboard part, which is in turn responsible for the largest amount of SBDE production. In fact, this deformation reduces it. Figure 7 shows the evolution of different parameters with the coupling iterations. Each of the curves is plot from the values taken at the optimization iterations performed by the aerodynamic optimizer. These plots clearly illustrate the effect of aeroelasticity. The rigid wing optimization is labelled as the "Coupling iteration 1". This first iteration carries the heaviest part of the optimization, because it runs the full way from the original wing to the optimized one. Approximately after 20 optimization iterations, the

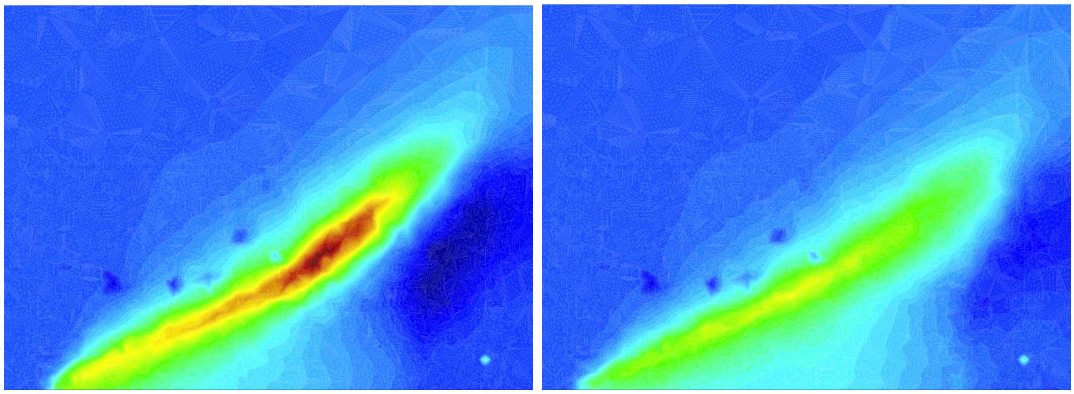

Figure 5: Dassault Aviation's Supersonic Business Jet. Non-coupled optimization of a rigid wing. Pressure distribution for a plane below the original and optimized wings, left and right respectively.

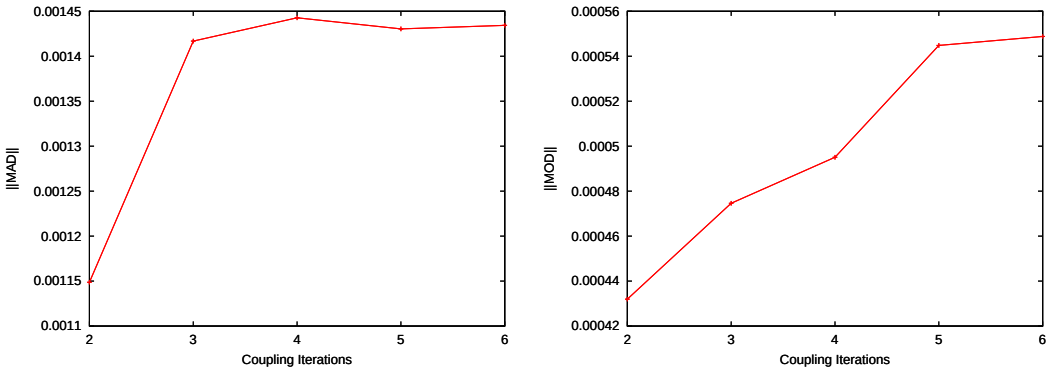

Figure 6: Dassault Aviation's Supersonic Business Jet. Convergence of the coupled algorithm. Evolution of the mean aeroelastic displacements (||MAD||) and the mean optimization displacements (||MOD||) with the coupling iterations.

lift is stabilized at the target value and the SBDE cost (defined as the third term of cost functional definition (1)) attains almost a 40% reduction. As said above, the incidence angle does not change because cambering is enough to recover the lift.

The next coupling iteration takes into account the aeroelastic deformation suffered by the optimized rigid wing. The convergence is in this case much faster. In five optimization iterations, the lift and SBDE terms of the cost functional stabilize. The lift is in this case regained by changing the incidence. In any case, this parameter is also stable after five iterations. This optimization stage has to recover about 20% of the lift, lost because of

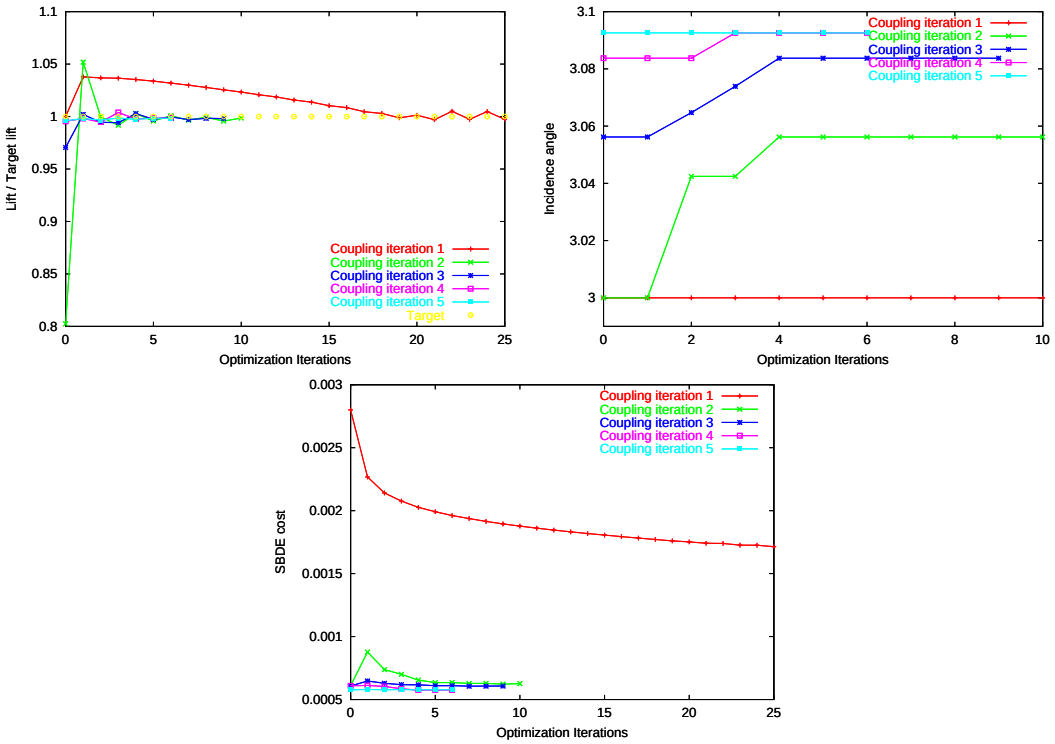

Figure 7: Dassault Aviation's Supersonic Business Jet. Convergence of the coupling algorithm. Evolution of different parameters with the coupling iterations.

the aeroelastic deformations. On the other hand, the SBDE has accordingly been reduced. Then, the objective is double: to recover the lift up to the value of the *rigid* optimized one and to further reduce the SBDE of the *deformed* wing. The SBDE reduction will not be so intense because most of the work has been done in the initial optimization, namely the rigid one. Basically, it can be said that the rest of the work consists in recovering the lift under the SBDE constraints. The next 4 coupling iterations have progressively smaller effect, converging to the lift target, effectively reducing the SBDE and stabilizing the incidence angle around 3.1°.

On the aeroelastic analysis side, we have observed that the loosely coupled scheme we used allows to obtain a convergent displacements norm, as seen in Figure 6. We name ||MAD|| the **Mean Aeroelastic Displacement Norm**, that is to say the L^2 norm of the aeroelastic displacements divided by the number of the moving surface nodes, which is equal to the dimension of the optimization parameters space. In the same figure, we have also

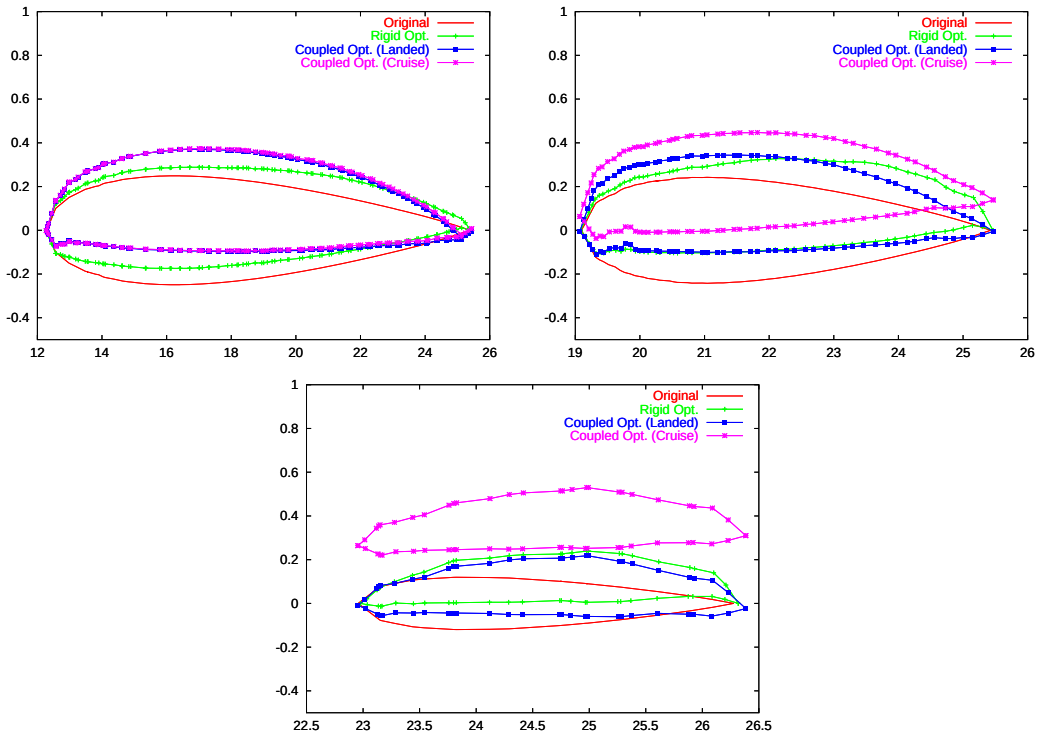

Figure 8: Dassault Aviation's Supersonic Business Jet. Optimized flexible wing. Clockwise: inboard, mid-wing and outboard cross-sectional cuts.

plotted the ||MOD||, the **Mean Optimization Displacements Norm** to see the scheme convergence and also to compare it with the ||MAD||.

The three optimized wing cross-sectional shapes of Figure 4 are again shown in Figure 8, but now including the plots corresponding to the coupling problem, in the "at rest" and "cruise" configuration. Recall that the configuration "at rest" is constructed from the "cruise" one (optimized or not) by substracting the aeroelastic displacements. In this way, the airfoil at rest compares to the rigid one. The optimized inboard airfoil now presents a larger cambering to gain part of the lift lost by the wing torsion and flexion. The flattened down side is due to the combination of the upper side spread-out (because the volume must be conserved locally for the corresponding section) and the SBDE reduction. At this wing location, the aeroelastic deformation is very small. The middle section is much more influenced by the deformations, and the negativetwist angle becomes apparent. From the comparison of both airfoils at rest, we observe how the method has compensated the twist effect (the wrinkled look is due to both the cutting process and the mesh coarseness). This

fact is even clearer in the outboard airfoil. The optimized down sides for both the cruise-coupled and the rigid problems present almost parallel shapes. Consequently, the at rest, coupled-optimized airfoil is very different from that of the rigid problem.

4.2 AGARD wing 445.6

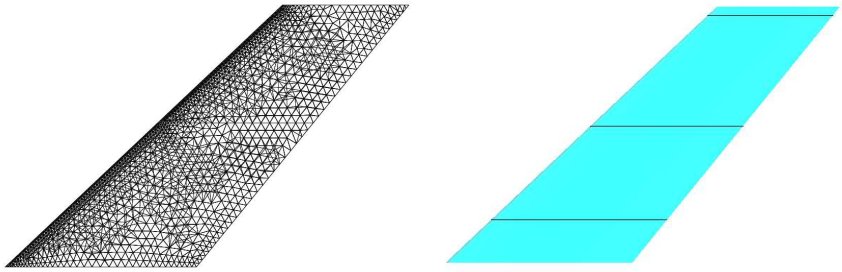

Figure 9: AGARD wing 445.6. Surface grid (left) and the three cross-sectional cuts.

We consider now the AGARD wing 445.6 whose geometry is described in details in [24]. The three dimensional unstructured CFD mesh contains 9505 nodes and 43973 tetrahedra. The surface wing (Figure 9) to optimize contains 5488 triangles and 2782 grid points, which is in turn the dimension of the parametrization space according to our CAD-free approach. The Mach number is set to 1.8 and the initial incidence angle is 3°.

4.2.1 Initial rigid optimization

In this first stage, we performed 20 optimization iterations. As in the previous example, this did not exhaust the optimization process for the rigid wing, but provides a good starting geometry for the coupled case. We have activated the VPGP strategy defined in Sec. 4.1.1, to keep constant the volume of each of 60 wingspan sections. Unlike the delta wing, the *rigid* AGARD wing produces basically the same shock strength all along its length. Therefore there is no outboard-inboard volume migration. However, this is very important for the *aeroelastic* case, and therefore the VPGP-by-sections solution is always adopted. We let the incidence angle vary according to (2), although for the rigid optimization the optimizer manages to preserve the lift only by cambering the wing. The α weight parameters in the cost functional (1) are set to $\alpha_1 = 10.0$, $\alpha_2 = 100.0$ and $\alpha_3 = 1.0$. The target lift and drag coefficients are respectively that of the original wing and half of it, evaluated at the initial incidence angle.

Figure 10 (left) shows the optimized wing mid-section compared to the original one. Figure 11 illustrates the effect of optimization on the SBDE by depicting the pressure distribution in a plane below the wing. Figure 10 (right) shows the pressure along a line below

the wing mid-section (Figure 9, right). Although the final converged state is not yet completely reached, because this first rigid optimization is no more than a first iterate for the coupled process, the tendency can be clearly seen. By minimizing the SBDE, the resulting shapes have flattened downwards faces and sharper leading edges. The SBDE, measured as the integral of the pressure below the wing, has diminished by rounding the main pressure peak and the following undershot. As reported in our previous works, this has the combined effect of (i) reducing the **pressure impulse**, (ii) reducing the initial pressure peak and (iii) introducing a **time delay** in the pressure rise. As shown in [11], this fact can be highlighted by computing the Euler flow around two 2-D profiles corresponding to the original and the optimized wings.

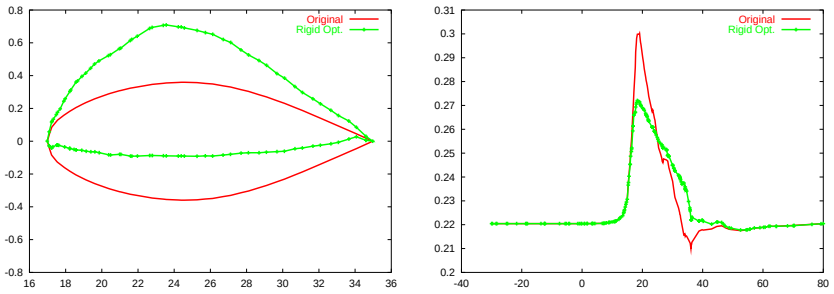

Figure 10: AGARD wing 445.6. Non-coupled optimization. Left, original and optimized (rigid) mid cross-sectional shapes or airfoils. Right, pressure below both airfoils.

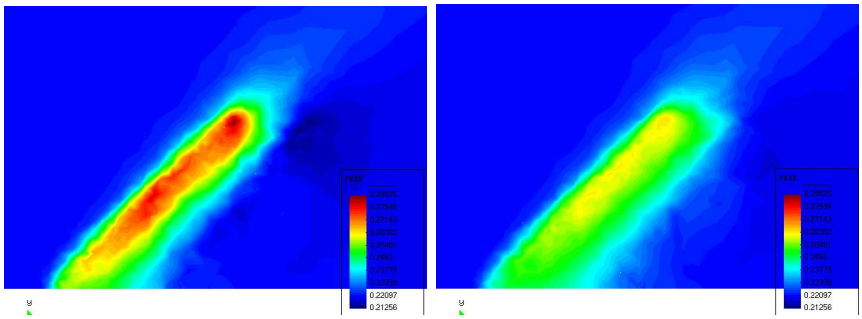

Figure 11: AGARD wing 445.6. Non-coupled optimization. Pressure distribution for a plane below the original and optimized (rigid) wings, left and right respectively.

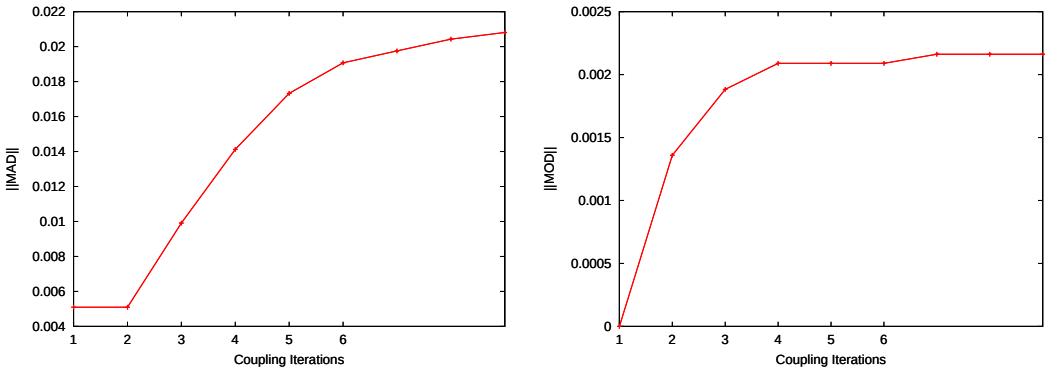

Figure 12: AGARD wing 445.6. Evolution of the mean aeroelastic displacements (||MAD||) and the mean optimization displacements (||MOD||) with the coupling iterations.

4.2.2 Optimization + Aeroelastic coupling

The optimized rigid wing of the previous section is taken as an initial guess for the coupled process. For the aeroelastic computation, we use a structural finite element model of the wing which contains 800 triangular composite shell elements and is based on the information given in [24]. This finite element model corresponds to a realistic wing designed for subsonic and transonic regimes.

Under supersonic conditions, the wing behavior becomes too elastic, undergoing large and rather unrealistic deformations. For this reason, this example is tougher than the SBJ delta wing and represents an appropriate test case to evaluate the robustness of the proposed method.

Figure 12 shows the evolution of the mean aeroelastic deformation norm and the mean optimization deformation norm. As in the previous case, these norms are stabilized after some coupling iterations. The plots in Figure 13 show the effects of the aeroelastic coupling in the optimization process. As in the SBJ's delta wing, the "target" lift is that of the original wing at the initial incidence angle 3°. The curve labelled as "Coupling iteration 1" corresponds to the initial rigid wing optimization. After each of the 9 coupling iterations, the target is progressively reached. This is done by the combined effect of cambering and incidence angle variation. The final incidence angle is almost triple of the initial one. This is the consequence of the large lost in lift due to the wing aeroelastic twist. The importance of this strong twist is obvious through the SBDE evolution (Figure 13, bottom). Additionally to the lift loss, the aeroelastic twist produces a strong reduction in SBDE, independently of the deformation coming from the optimization method. Then, the algorithm tries to recover the lift while keeping the SBDE reduction. It is obvious that for this highly deformable wing, a much larger incidence angle is needed in order to recover the lift, which rises in turn the SBDE production. This results in a final SBDE that is very close to that of the

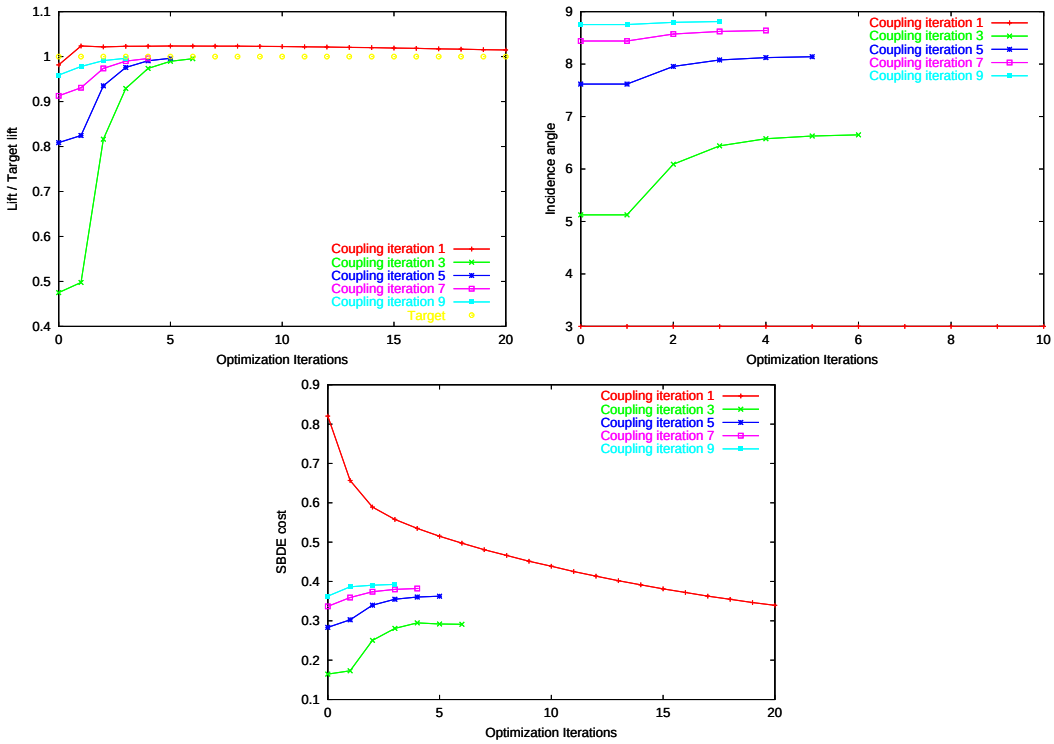

Figure 13: AGARD wing 445.6. Evolution of different parameters with the coupling iterations.

rigid optimized wing, with a rather different geometry at rest. In any case, the relative weights of these effects are controlled by the α's set. We have preferred to keep them equal to those of the delta wing for comparison purposes. The extreme flexibility of the wing at this supersonic regime is seen in Figure 14.

5 Concluding remarks

In this paper, we have proposed a method for the optimization of flexible wings which undergo deformations by the action of a flow.

This is done following a two-step iterative procedure.

At each coupling iteration, an aeroelastic analysis is followed by an aerodynamic optimization.

The aeroelastic analysis is based on a classical loosely-coupled method. The shape optimizer combines a "CAD-free" approach with transpiration conditions to handle the opti-

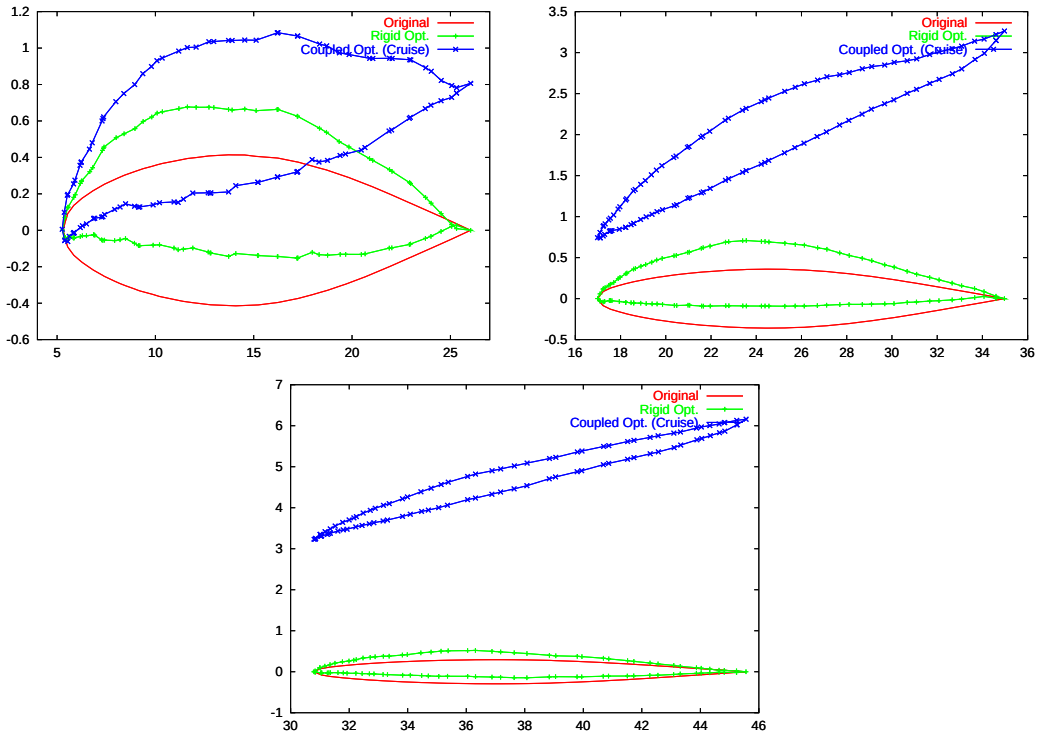

Figure 14: AGARD wing 445.6. Optimized wing. Clockwise: inboard, mid-wing and outboard cross-sectional cuts.

mization deformations. It computes an optimized shape from the aeroelastic deformed wing produced by the first step. Both steps are connected through a controlled deformation of the volumic mesh to adapt it to the optimized surfaces.

The proposed approach allows the coupling of existing modules without a complex and costly development phase. In contrast to a fully coupled optimization algorithm, the management of a three-field state system and thus a three-field adjoint one is avoided. No sensitivities are computed on the aeroelastic side.

The proposed approach is also an efficient one. Through two different examples, we have observed a convergent behaviour of the scheme, which is reached after no more than 10 coupling iterations.

For demonstration, it is applied to flexible wings for the sonic boom reduction while preserving good aerodynamic properties.

The examples shown represent two very significative ones. The first one is a double-delta wing for a projected supersonic business jet. The obtained optimized shapes present very different longitudinal sections, according to their relative wing-span position. The second

one is an AGARD 445.6 wing submitted to very large deformations. Due to its extreme deformation conditions this example push the limits of the scheme, proving it to be very robust and reliable. In both cases, the influence of the aeroelastic deformations on the sonic boom optimization process is clearly shown . This fact cannot be neglected at all, particularly when different flight regimes of a supersonic jet are considered. The effect is quite obvious when both rigid and coupled "at rest" optimized shapes are compared.

The shapes, so-obtained, are evaluated with the corresponding mesh deformation, which means that the transpiration approximation does not influence the evaluation of the flow and its performances, but only the identification of an optimum.

Furthermore, the proposed method has a good potentiallility to be extended to the case where a more accurate optimization loop, relying on mesh deformation in place of transpiration, is chosen in place of the module used in our study.

These features tend to show that the proposed method is well-adapted to the cooperation between departmental tools in industrial context (local grid computing). Methods of this kind open the door to accurate multipoint optimization thanks to a complete, but not communication-intensive coupling, in a multidisciplinary cooperative optimization.

Acknowledgments

This work was supported by Comité d'Orientation Supersonique of French Ministery of Research. The authors are also grateful to CINES (Centre Informatique National de l'Enseignement Supérieur) for providing computational facilities. We thank Stephen Wornom for kindly proof reading this paper.

References

[1] J. SOBIESZCZANSKI-SOBIESKI and R.T. HAFTKA. Multidisciplinary aerospace design optimization: survey of recent developments. *Structural Optimization*, 14(1), 1997.

[2] AIAA Technical Committee for MDO. Current state of the art of multidisciplinary design optimization. AIAA White Paper, September 1991.

[3] A.C. TAYLOR, L.L. GREEN, P.A. NEWMAN, and M.M. PUTKO. Some advanced concepts in discrete aerodynamic sensitivity analysis. *AIAA Paper*, 2001-2529:1–10, 2001.

[4] J.C. NEWMAN, W.K. ANDERSON, and D.L. WHITFIELD. Multidisciplinary sensitivity derivatives using complex variables. Technical Report - CFD Laboratory - Mississippi State University MSSU-COE-ERC-98-08, July 1998.

[5] A.A. GIUNTA. Sensitivity analysis for coupled aero-structural systems. NASA Technical Report NASA/TM-1999-209367, August 1999.

[6] J. SOBIESZCZANSKI-SOBIESKI. Sensitivity of complex, internally coupled systems. *AIAA J.*, 28(1):153–160, 1990.

[7] K. MAUTE, M. NIKBAY, and C. FARHAT. Sensitivity analysis and design optimization of three-dimensional non-linear aeroelastic systems by the adjoint method. *Int. J. Numer. Meth. Engng.*, 56:911–933, 2003.

[8] A.A. GIUNTA and J. SOBIESZCZANSKI-SOBIESKI. Progress toward using sensitivity derivatives in high-fidelity aeroelastic analysis of a supersonic transport. *AIAA Paper*, 98-4763:1–13, 1998.

[9] B. MOHAMMADI and O. PIRONNEAU. *Applied shape optimization for fluids.* Clarendon Press - Oxford, 2001.

[10] C. FARHAT, M. LESOINNE, and N. MAMAN. Mixed explicit/implicit time integration of coupled aeroelastic problems: three-field formulation, geometric conservation and distributed solution. *Int. J. Num. Meth. Fluids.*, 21:807–835, 1995.

[11] M. VAZQUEZ, B. KOOBUS, and A. DERVIEUX. Aerodynamical and sonic boom optimization of a supersonic aircraft. Technical Report RR-4520, INRIA, 2002. http://www-sop.inria.fr/rapports/sophia/RR-4520.html.

[12] M. VAZQUEZ, B. KOOBUS, and A. DERVIEUX. Multilevel optimization of a supersonic aircraft. *Submitted, also INRIA Technical report*, (RR-4520), 2002. http://www-sop.inria.fr/rapports/sophia/RR-4520.html.

[13] R. SEEBAS and B. ARGROW. Sonic boom minimization revisited. *AIAA Paper*, 98-2956:1–13, 1998.

[14] C. FARHAT. High performance simulation of coupled non-linear transient aeroelastic problems. AGARD Report R-807, October 1995. Special Course on Parallel Computing in CFD.

[15] C. FARHAT and M. LESOINNE. On the accuracy, stability and performance of the solution of three-dimensional non-linear transient aeroelastic problems by partitioned procedures. *AIAA paper 96-1388*, April 18-19, 1996.

[16] C. FARHAT, C. DEGAND, B. KOOBUS, and M. LESOINNE. Torsional springs for two-dimensional dynamic unstructured fluid meshes. *Comput. Meths. Appl. Mech. Engrg.*, 163:231–245, 1998.

[17] J. REUTHER and A. JAMESON. Aerodynamic Shape Optimization of Wing and Wing-Body Configurations Using Control Theory. AIAA Paper 95-0123, 1995. 33rd Aerospace Sciences Meeting and Exhibit.

[18] A. DERVIEUX, S. LANTERI, J.M. MALE, N. MARCO, N. ROSTAING-SCHMIDT, and B. STOUFFLET. New technologies for advanced three-dimensional optimum shape design in aeronautics. *Int. J. Num. Meth. Fluids.*, 30:179–191, 1999.

[19] F. COURTY, A.DERVIEUX, B. KOOBUS, and L. HASCOET. Reverse automatic differentiation for optimum design: from adjoint state assembly to gradient computation. Technical Report RR-4363, INRIA, 2002. http://www-sop.inria.fr/rapports/sophia/RR-4363.html.

[20] N. MARCO and A. DERVIEUX. Multilevel parametrization for aerodynamical optimization of 3D shapes. *Finite Elements in Analysis and Design*, 26:259–277, 1997.

[21] B. MOHAMMADI. Optimization of aerodynamic and acoustic performances of supersonic civil transports. In *Center for Turbulence Research. Proceedings of the Summer Program 2002*, 2002.

[22] J. D. ANDERSON. *Introduction to Flight.* Mc. Graw - Hill, 2000.

[23] C. HELD and A. DERVIEUX. One-shot airfoil optimisation without adjoint. *Computers and Fluids*, 31(8):1015–1049, 2002.

[24] E.C. YATES. AGARD standard aeroelastic configuration for dynamic response, candidate configuration i. - wing 445.6. *NASA TM-100492*, 1987.

Unité de recherche INRIA Sophia Antipolis
2004, route des Lucioles - BP 93 - 06902 Sophia Antipolis Cedex (France)

Unité de recherche INRIA Futurs : Parc Club Orsay Université - ZAC des Vignes
4, rue Jacques Monod - 91893 ORSAY Cedex (France)
Unité de recherche INRIA Lorraine : LORIA, Technopôle de Nancy-Brabois - Campus scientifique
615, rue du Jardin Botanique - BP 101 - 54602 Villers-lès-Nancy Cedex (France)
Unité de recherche INRIA Rennes : IRISA, Campus universitaire de Beaulieu - 35042 Rennes Cedex (France)
Unité de recherche INRIA Rhône-Alpes : 655, avenue de l'Europe - 38334 Montbonnot Saint-Ismier (France)
Unité de recherche INRIA Rocquencourt : Domaine de Voluceau - Rocquencourt - BP 105 - 78153 Le Chesnay Cedex (France)

Éditeur
INRIA - Domaine de Voluceau - Rocquencourt, BP 105 - 78153 Le Chesnay Cedex (France)
http://www.inria.fr
ISSN 0249-6399